JOURNAL OF THE AMERICAN CHEMICAL SOCIETY

pubs.acs.org/JACS

Article

Extension and Fusion of Cyclic Polyantimony Units

Yu-He Xu, Wen-Juan Tian, Jing-Ying Sun, Manfred Scheer,* and Zhong-Ming Sun*

Cite This: https://doi.org/10.1021/jacs.4c03843

Read Online

ACCESS | Metrics & More | Article Recommendations | Supporting Information

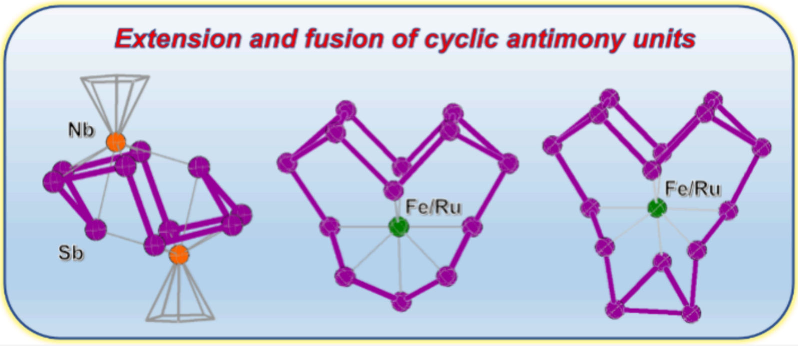

ABSTRACT: The synthesis and characterization of a series of polyantimony anionic clusters are reported. The products $[(NbCp)_2Sb_{10}]^{2-}$, $[MSb_{13}]^{3-}$ (M = Ru/Fe), and $[MSb_{15}]^{3-}$ (M = Ru/Fe) were isolated as either K(18-crown-6) or K([2.2.2]-crypt) salts. The Sb_{10} ring contained in the $[(NbCp)_2Sb_{10}]^{2-}$ cluster can be viewed as an extension of two envelope-like *cyclo*-Sb_5 units and represents by far the largest monocyclic all-antimony species. The clusters $[MSb_{13}]^{3-}$ and $[MSb_{15}]^{3-}$ (M = Ru/Fe) illustrate the variability of crown-like Sb_8 ring motifs and reveal the fusion of different antimony fragments featuring unique Sb−Sb chain-like units. The reported synthetic approaches involve the fabrication of a variety of distinctive polyantimony anionic clusters, enhancing our understanding of the coordination chemistry of heavier group 15 elements.

■ INTRODUCTION

The tendency for disproportionation processes and facile structural rearrangements of polyantimonides greatly enriches the types of antimony clusters.[1,2] In addition to the ability to form chain-like units, another notable characteristic of antimony atoms is their ability to form ring units.[3,4] Several cyclic structural motifs that can be classified into three categories have been identified (Scheme 1). The first type is represented by planar cyclic units that include three-membered, four-membered, and five-membered rings in which, e.g., the $[Sb_4]^{2-}$ anion can exist by itself and that were isolated from solutions of A_5Sb_4 (A = K, Rb, Cs).[5] In contrast, the Sb_3 and Sb_5 rings must be coordinated to a metal atom or organic groups for stabilization.[6−8] The second type is represented by folded monocyclic units, mainly consisting of hexagonal and octagonal rings. The $[Sb_6]^{4-}$ unit includes two configurations, a boat-like and chair conformer.[9,10] The $[Sb_8]^{8-}$ anion exhibits a crown-like structure and can either exist in liquid ammonia or be coordinated by a transition metal such as Nb or Mo at the center of the ring, allowing it to be isolated from conventional solvents.[11−13] In addition, polycyclic structural units contain more antimony atoms. The norbornadiene-like $[Sb_7]^{3-}$ and polycyclic $[Sb_{10}]^{2-}$ and $[Sb_{11}]^{3-}$ units (composed of four-/five-membered and solely five-membered rings, respectively) can be extracted from the corresponding Zintl phases.[5,14−19] In contrast, the realgar-type $[Sb_8]^{4-}$ unit requires the coordination of four organometallic moieties by four twofold-connected Sb atoms for stabilization.[7,20−24] In contrast to the lighter congeners (P and As) where polypnictogen ligands and cages can be extended by joining two basic cyclic units into a chain-like structure through a Pn−Pn single bond (Pn = pnictogen),[25−27] such an extension method is almost unknown for antimony. There are very few relevant reports, with, e.g., a silyl group-protected bicycle R_6Sb_8 (R= $(Me_3Si)_2CH$), in which two Sb_4 rings are connected by a Sb−Sb single bond.[7] Another possibility is to aggregate antimony entities by rare earth or transition metals, like in $[Ln(\eta^4\text{-}Sb_4)_3]^{3-}$ (Ln = La, Y, Ho, Er, Lu), where three *cyclo*-Sb_4 units are combined by one Ln^{3+} ion with long Sb···Sb contacts between the *cyclo*-Sb_4 rings.[28] A similar example is the anion $[(ZnSb_6)_2]^{4-}$, which represents a new type of coupled norbornadiene subunits.[29] These studies demonstrated the aggregation of Sb fragments without expanding the cyclic Sb units. Herein, we report the synthesis of novel polycyclic Sb_n

Received: March 18, 2024
Revised: May 16, 2024
Accepted: May 16, 2024

Scheme 1. (a−c) Selected Examples of *cyclo*-Sb_n Ligand Complexes; (d) This Work

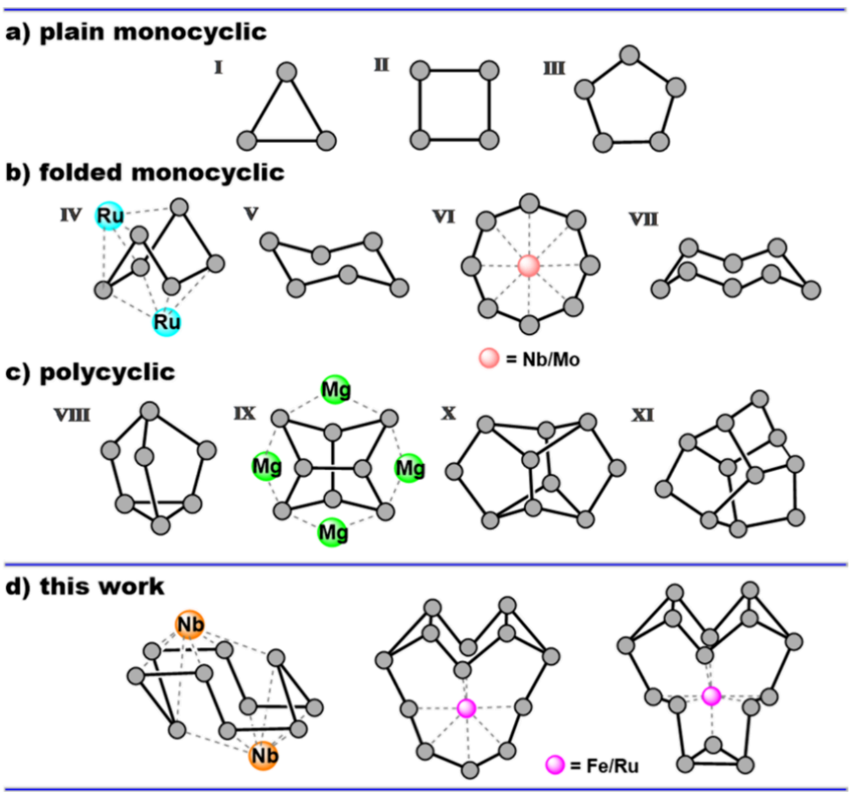

units containing unprecedented Sb−Sb chain moieties to extend Sb_n cluster cores, such as the strongly folded *cyclo*-Sb_{10} ligand within the compound $[K(2.2.2\text{-crypt})]_2[(NbCp)_2Sb_{10}]$ (**1**), which represents the largest monocyclic all-antimony species known to date. In addition, butterfly-shaped clusters $[MSb_{13}]^{3-}$ (M = Ru/Fe) exist in $[K(18\text{-crown-6})]_3[RuSb_{13}]\cdot 5.5en$ (**2**) and $[K(18\text{-crown-6})]_3[FeSb_{13}]$ (**4**), where the antimony unit can be regarded as a recombination of one *cyclo*-Sb_8 ring and half an $[M@Sb_8]$ unit. Moreover, their evenly extended Sb_{15} form in $[K(18\text{-crown-6})]_3[RuSb_{15}]\cdot en$ (**3**) and $[K(18\text{-crown-6})]_3[FeSb_{15}]\cdot 5en$ (**5**) is displayed as well.

■ RESULTS AND DISCUSSION

By reacting K_6ZnSb_5 with $NbCp_4$ in the presence of [2.2.2]crypt in an ethylenediamine (en) solution at room temperature (r.t.), black rod-like crystals of **1** were obtained after 1 week (Scheme 2) on the wall of the tube. Compound **2** was prepared by the reaction of K_5Sb_4 with $Ru(PPh_3)_3Cl_2$ in a mixture of en, 18-crown-6, and toluene. The reaction mixture was stirred for 3 h at 60 °C, and black block-like crystals of **2** were isolated after storage for 2 weeks. Compound **3** could also be prepared under similar reaction conditions to those employed for **2** but required additional heating to 90 °C for 1 h. The reaction of K_3Sb_7 and 18-crown-6 with $Fe(OCPh_3)_2thf_2\cdot en$ at r.t. for 4 h yields compound **4**. When the reaction conditions were changed from r.t. to 70 °C, product **5** was obtained within 2 h. In general, the corresponding 13-atom clusters and 15-atom clusters can be synthesized from the same starting material; however, the 15-atom clusters require a higher reaction temperature compared to the 13-atom ones. Interestingly, when the reaction mixtures of compounds **2** and **4** were stored for 1 week, crystals of **3** and **5**, respectively, were formed, whereas the number of crystals of **2** and **4** decreased. However, these conversions need the mother liquor of the reaction mixtures and are not possible starting from the isolated products **2** (**4**) in new solvent mixtures.

Crystals of **1**−**3** and **5** were suitable for single-crystal X-ray diffraction analysis, but despite numerous attempts, it was not possible to obtain single crystals of compound **4** with sufficient quality for full structural characterization. However, it is possible to discern the structure of the heavy atom core, which is isomorphic to the $[RuSb_{13}]^{3-}$ cluster. Fortunately, the ESI-MS spectra of crystals of **1**−**5** dissolved in acetonitrile (MeCN) or dimethylformamide (DMF) provide a plethora of information. Complete cluster fragments of all five compounds were found in the negative ion mode mass spectra, which showed prominent peaks for the parent ions at m/z = 1532.9345 ($[(NbCp)_2Sb_{10}]^-$), m/z = 1683.6162 ($[RuSb_{13}]^-$), m/z = 1927.4389 ($[RuSb_{15}]^-$), m/z = 1637.6373 ($[FeSb_{13}]^-$), and m/z = 2184.5688 ($[K(18\text{-c-6})\ FeSb_{15}]^-$) (Figure 1). The complete composition of the $[FeSb_{13}]^{3-}$ cluster is maintained

Scheme 2. Syntheses of Compounds 1−5

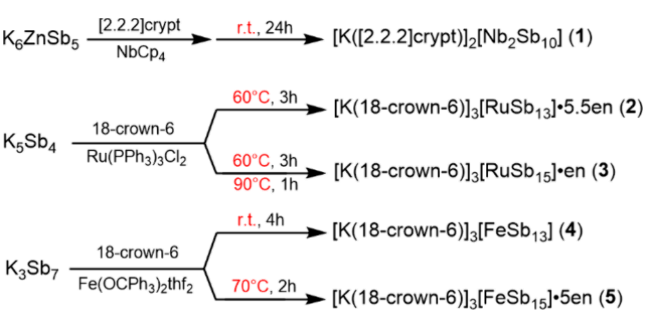

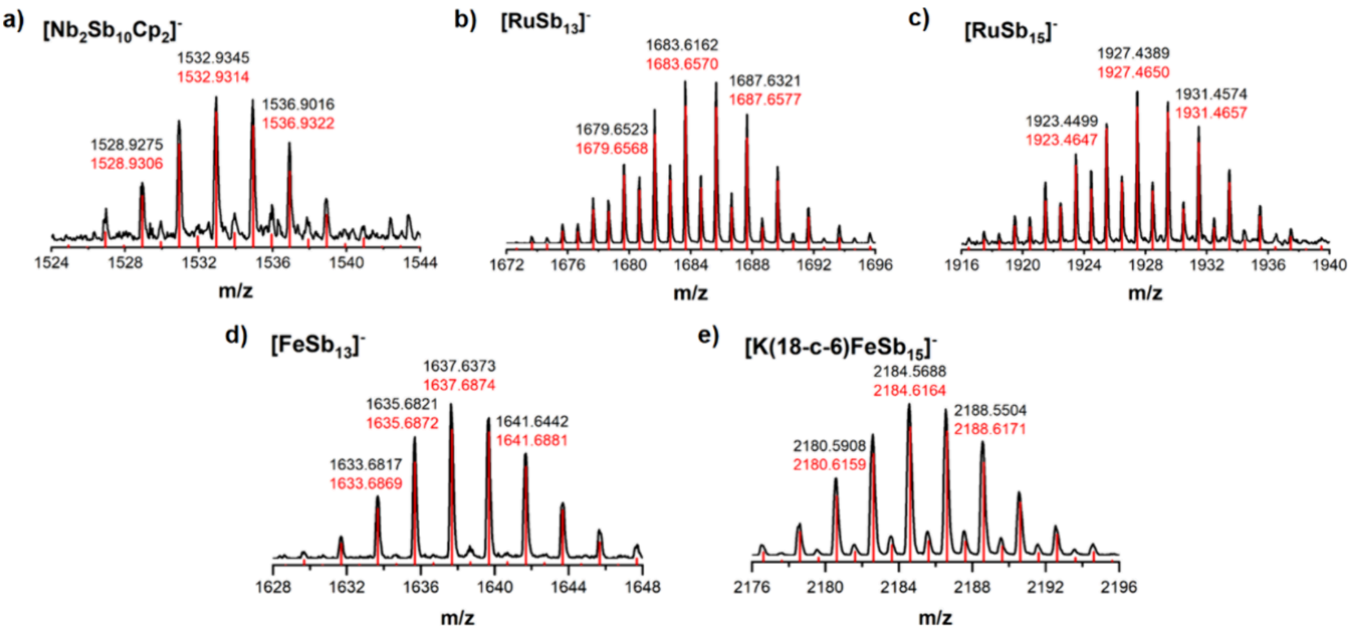

Figure 1. Negative ion mode ESI mass peaks corresponding to (a) $[(NbCp)_2Sb_{10}]^-$, (b) $[RuSb_{13}]^-$, (c) $[RuSb_{15}]^-$, (d) $[FeSb_{13}]^-$, and (e) $[K(18\text{-}c\text{-}6)\,FeSb_{15}]^-$. The experimental mass distributions are depicted in black, and the theoretical masses of the isotope distributions are shown in red.

even under rather harsh MS conditions, which further indicates the existence of the $[FeSb_{13}]^{3-}$ core.

Compound **1** crystallizes in the triclinic space group *P*-1 and possesses one $[(NbCp)_2Sb_{10}]^{2-}$ anionic cluster and two $[K(crypt\text{-}222)]^+$ cations in the asymmetric unit. As shown in Figure 2, the structure of the $[(NbCp)_2Sb_{10}]^{2-}$ cluster can be

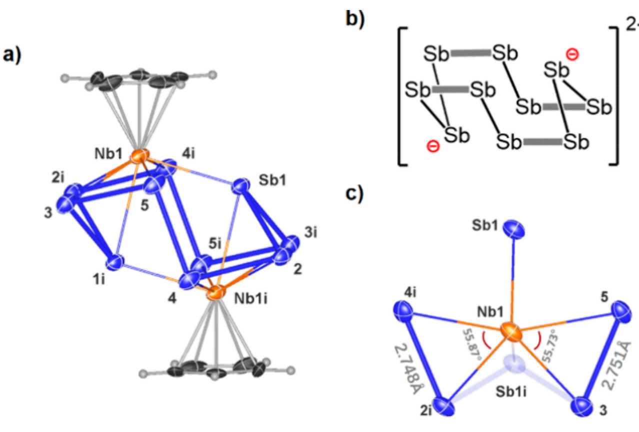

Figure 2. (a) Molecular structure of the $[(NbCp)_2Sb_{10}]^{2-}$ anion in **1** (generated via the symmetric code of #1-*x*, 1-*y*, 1-*z*) drawn with thermal ellipsoids at the 50% level. (b) The *cyclo*-Sb_{10} unit of $[(NbCp)_2Sb_{10}]^{2-}$. (c) The coordination mode of an Nb atom in the $[(NbCp)_2Sb_{10}]^{2-}$ cluster.

regarded as a folded Sb_{10} ring coordinated by two NbCp fragments. The Sb_{10} ring represents the largest monocyclic Sb_n unit reported thus far. The Sb−Sb bonds in the Sb_{10} ring are arranged alternately with longer and shorter bond lengths. The longer Sb−Sb bonds are between 2.7843 and 2.8177 Å, which falls within the range of typical Sb−Sb single bonds, while the shorter Sb−Sb bonds (2.7481 to 2.7512 Å) are between single and double bonds.[5,19,23,24] Taking the reported isostructural P_{10} ring as a reference, there are four P═P double bonds and two negative charges carried by the *cyclo*-P_{10} unit, which can be located at the two bent atoms of the folded ring.[30] The two negative charges on the Sb_{10} ring are also located in the same region, which confirms the Zintl−Klemm concept (Figure 2b), namely, that the twofold-connected Sb atom carries a negative charge. In an alternative resonance form, shorter Sb−Sb bonds can be viewed as possessing Sb═Sb double bond characteristics. The Nb−Sb bonds in $[(NbCp)_2Sb_{10}]^{2-}$ are in the range of 2.8699−2.9944 Å, which is slightly longer than those in $[Nb@Sb_8]^{3-}$ (2.8393−2.9332 Å) and in organometallic complexes containing a CpNb-Sb fragment (2.8929 Å).[12,31]

Compound **2** crystallizes in the triclinic space group *P*-1, while compounds **3** and **5** crystallize in the monoclinic space group $P2_1/c$. The clusters $[RuSb_{13}]^{3-}$ and $[RuSb_{15}]^{3-}$ are isostructural with $[FeSb_{13}]^{3-}$ and $[FeSb_{15}]^{3-}$, respectively, and in the following, the structures of $[RuSb_{13}]^{3-}$ and $[RuSb_{15}]^{3-}$ will be mainly discussed as representatives (Figure 3). The upper part of the $[RuSb_{13}]^{3-}$ cluster can be viewed as a squashed crown-like Sb_8 ring. Compared with the S_8-like $[Sb_8]^{8-}$ anion present in ammonia,[11] the connection of the Sb5−Sb6 and Sb9−Sb10 atoms in the $[RuSb_{13}]^{3-}$ cluster shortens the length of one of the axes and changes the ratio of the long axis to the short axis of the Sb_8 ring from 1.02 to 1.98 (Sb4···Sb11/Sb7···Sb8). The bond angles of the *cyclo*-Sb_8 unit in the $[RuSb_{13}]^{3-}$ cluster are approximately 100° and between $[Sb_8]^{8-}$ (115°) and $[Nb@Sb_8]^{3-}$ (87°), which suggests that a less puckered shape is favored by uncoordinated crown molecules. The atoms Sb1−Sb3 and Sb12−Sb13 together with the embedded Ru atom collectively form a structural fragment similar to one-half of the $[Nb@Sb_8]^{3-}$ cluster (Figure 3a,c).[12] The coordination angles between the Sb atoms and the central transition metal atom lie in a narrow range of 61.39−62.08°, slightly larger than those of $[Nb@Sb_8]^{3-}$ (57.06−60.02°). The top part of the $[RuSb_{15}]^{3-}$ cluster is almost identical to that of the $[RuSb_{13}]^{3-}$ cluster. The difference lies in the bottom part, where three atoms of the $[RuSb_{13}]^{3-}$ cluster are replaced by a trigonal prismatic unit missing one Sb edge. All Sb−Sb bonds in the $[RuSb_{13}]^{3-}$ cluster are between 2.7641 and 2.8966 Å, comparable to those in the $[RuSb_{15}]^{3-}$ cluster, and are both typical of two-center two-electron single

https://doi.org/10.1021/jacs.4c03843
J. Am. Chem. Soc. XXXX, XXX, XXX−XXX

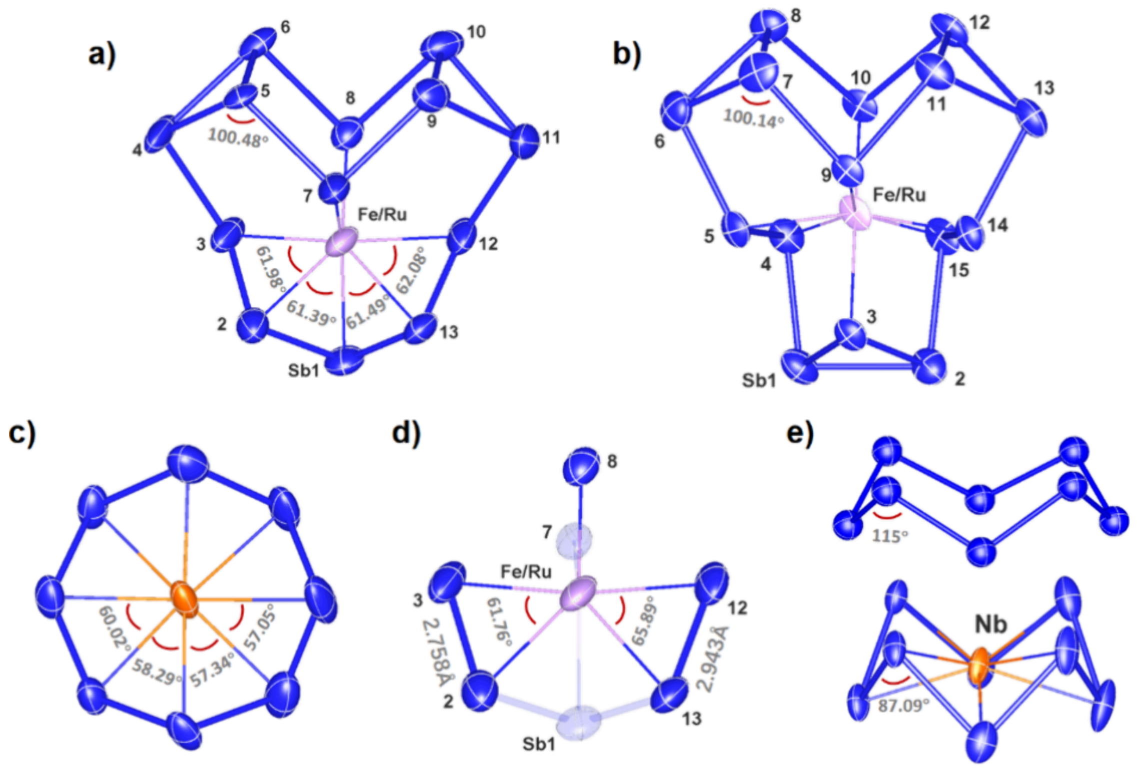

Figure 3. (a) Molecular structures of the $[MSb_{13}]^{3-}$ (M = Fe/Ru) anions in the solid state drawn with thermal ellipsoids (50% level). (b) Molecular structures of the $[MSb_{15}]^{3-}$ (M = Fe/Ru) anions in the solid state drawn with thermal ellipsoids (50% level). (c) Molecular structure of the $[Nb@Sb_8]^{3-}$ anions in the solid state drawn with thermal ellipsoids (50% level). (d) The coordination mode of Fe/Ru atoms in the clusters $[MSb_{13}]^{3-}$ and $[MSb_{15}]^{3-}$ (M = Fe/Ru). (e) The side view of $[Sb_8]^{8-}$ and $[Nb@Sb_8]^{3-}$.[11,12]

bonds. Compared with the Ru–Sb bonds in the cluster $[RuSb_{15}]^{3-}$ (2.5964–2.7200 Å), the Ru–Sb bond lengths in $[RuSb_{13}]^{3-}$ fall into a larger range of 2.5535–2.7347 Å, thus being shorter than those of $[Sb_6(RuCp^*)_2]^{2-}$ (2.6848–2.7903 Å).[10] There are only a limited number of examples for which to compare Fe–Sb bonds with literature data because only a few organometallic compounds exist, such as $[\{Fe_3(CO)_9\}\{\mu_3\text{-}SbFe(CO)_2Cp''\}_2]$ (2.5075–2.5607 Å) and $[Fe_2Sb(CO)_5Cp]_4$ (2.6136–2.6581 Å), which are comparable to those in the cluster $[FeSb_{15}]^{3-}$ (2.5251–2.6769 Å).[32,33] It is worth noting that some of the coordination modes of the metal-Sb_n frameworks show similarities between the cluster $[(NbCp)_2Sb_{10}]^{2-}$ and the clusters $[MSb_{13}]^{3-}$ and $[MSb_{15}]^{3-}$ (M = Fe/Ru). As shown in Figures 2c and 3d, one central atom is coordinated by two Sb–Sb units and one Sb atom. The coordination angles of the $[(NbCp)_2Sb_{10}]^{2-}$ cluster are 55.87 and 55.73°, respectively, which are slightly smaller than those of the remaining four clusters (61.76 and 65.89° a.v.).

Density functional theory (DFT) computations utilizing the experimentally observed structures and charges of the $[(NbCp)_2Sb_{10}]^{2-}$, $[RuSb_{13}]^{3-}$, and $[RuSb_{15}]^{3-}$ clusters demonstrate energy gaps of 2.41, 2.52, and 2.85 eV, respectively, between the highest occupied molecular orbital (HOMO) and the lowest unoccupied molecular orbital (LUMO) (Figure 4).[34,35] Detailed analyses of natural atomic orbitals show the participation of Ru in $[RuSb_{13}]^{3-}$ and $[RuSb_{15}]^{3-}$, with the composition being 11.1 and 4.6% for the corresponding HOMO, respectively. Moreover, the major contribution comes from the d electrons of the Ru atom. Meanwhile, the Nb atom (2.6%) also contributes to the HOMO of $[(NbCp)_2Sb_{10}]^{2-}$. Additionally, the surrounding Sb atoms in these clusters make

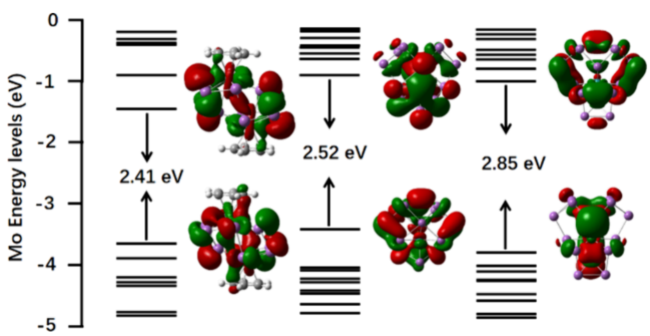

Figure 4. Molecular orbital diagram of the $[(NbCp)_2Sb_{10}]^{2-}$, $[RuSb_{13}]^{3-}$, and $[RuSb_{15}]^{3-}$ clusters (from left to right); the energies of the HOMO/LUMO gaps are given.

the major contribution to the HOMO (Table S6) and along with the participation of Ru and Nb, giving rise to the stability of these clusters.

Further investigations of the bonding characteristics of the $[(NbCp)_2Sb_{10}]^{2-}$, $[RuSb_{13}]^{3-}$, and $[RuSb_{15}]^{3-}$ clusters were conducted using the adaptive natural density partitioning (AdNDP) method.[36,37] The $[RuSb_{13}]^{3-}$ cluster has a total of 76 valence electrons, with each antimony (Sb) atom contributing five valence electrons and one ruthenium (Ru) atom providing eight valence electrons. Considering the three negative charges of the cluster, there are a total of 76 valence electrons. The distribution of these 76 valence electrons reveals that in the $[RuSb_{13}]^{3-}$ cluster, each Sb atom has an s-type lone pair of electrons; the central Ru atom has two d-type lone pairs of electrons. Additionally, each Sb–Sb bond features a 2c–2e Sb–Sb σ bond, and each Ru–Sb bond contains a 2c–2e Ru–

https://doi.org/10.1021/jacs.4c03843
J. Am. Chem. Soc. XXXX, XXX, XXX–XXX

Sb σ bond. In the $[RuSb_{15}]^{3-}$ cluster, a similar bonding pattern is observed, with the distinction that there are s-type lone pairs of electrons on 15 Sb atoms and 19 2c−2e Sb−Sb σ bonds. The $[(NbCp)_2Sb_{10}]^{2-}$ cluster (Figure 5) comprises a total of 60 valence electrons. Each of the Nb and Sb atoms possesses a pair of 5 s lone electrons, contributing to a cumulative count of 24 electrons. Notably, two Nb atoms engage in the formation of six Nb−Sb 2c−2e σ bonds with each of the three closely spaced Sb atoms. The molecular architecture is further stabilized by the creation of 10 Sb−Sb 2c−2e σ bonds between adjacent Sb atoms, establishing the peripheral structural framework of the cluster. The remaining four electrons participate in the establishment of two 8c−2e delocalized bonds, which indicates the multicenter delocalization bonds of each Nb_2Sb_6 part. The delocalized 8c−2e bond indicates the interaction between Nb and the surrounding six Sb atoms, certainly including the interaction between Nb and Sb4 and Sb5 (Figure 2c), plus the formation of the localized Nb−Sb1 bond, which makes the Nb atom deviate from the middle of the Sb═Sb double bond but more shifted toward Sb4−Sb5.

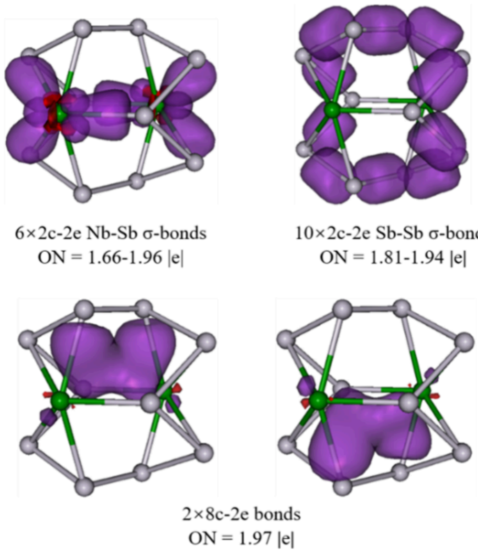

Figure 5. Chemical bonding analysis of the $[(NbCp)_2Sb_{10}]^{2-}$ cluster by the AdNDP method.

CONCLUSIONS

In summary, we were able to show that by starting from Sb-containing Zintl phases in the reaction with organometallic transition metal complexes, the unprecedented polyantimony anions $[(NbCp)_2Sb_{10}]^{2-}$, $[MSb_{13}]^{3-}$ (M = Ru/Fe), and $[MSb_{15}]^{3-}$ (M = Ru/Fe) were isolated. The $[(NbCp)_2Sb_{10}]^{2-}$ cluster comprises a folded Sb ring with alternating Sb−Sb bond lengths and thus represents the largest monocyclic all-Sb species reported thus far. The $[MSb_{13}]^{3-}$ and $[MSb_{15}]^{3-}$ (M = Ru/Fe) clusters exhibit strong correlations in both the experimental synthesis and structural topology. Whereas the upper halves of the structures of the clusters $[MSb_{13}]^{3-}$ (M = Ru/Fe) and $[MSb_{15}]^{3-}$ (M = Ru/Fe) are identical, their bottom parts feature different unique Sb−Sb chain moieties. Thus, with these first examples, Sb chemistry closes the gap in the chemistry of the lighter congeners P and As. After allowing the mother liquor of crystals **2**(**4**) to stand for an additional week, the formation of compounds **3**(**5**) was observed, revealing the thermodynamically greater stability of the $[MSb_{15}]^{3-}$ clusters. This series of compounds demonstrates the fusion and growth processes of antimony clusters, highlighting the diverse coordination patterns of Sb.

ASSOCIATED CONTENT

Supporting Information

The Supporting Information is available free of charge at https://pubs.acs.org/doi/10.1021/jacs.4c03843.

Experimental procedures, crystallographic supplementation, energy-dispersive X-ray (EDX) spectroscopic analysis, and quantum-chemical studies (PDF)

Accession Codes

CCDC 2334097, 2334104, 2334106, and 2334151 contain the supplementary crystallographic data for this paper. These data can be obtained free of charge via www.ccdc.cam.ac.uk/data_request/cif, or by emailing data_request@ccdc.cam.ac.uk, or by contacting The Cambridge Crystallographic Data Centre, 12 Union Road, Cambridge CB2 1EZ, UK; fax: +44 1223 336033.

AUTHOR INFORMATION

Corresponding Authors

Manfred Scheer − *Institute of Inorganic Chemistry, University of Regensburg, Regensburg 93040, Germany;* orcid.org/0000-0003-2182-5020; Email: Manfred.Scheer@chemie.uni-regensburg.de

Zhong-Ming Sun − *State Key Laboratory of Elemento-Organic Chemistry, Tianjin Key Lab for Rare Earth Materials and Applications, School of Materials Science and Engineering, Nankai University, Tianjin 300350, China;* orcid.org/0000-0003-2894-6327; Email: sunlab@nankai.edu.cn

Authors

Yu-He Xu − *State Key Laboratory of Elemento-Organic Chemistry, Tianjin Key Lab for Rare Earth Materials and Applications, School of Materials Science and Engineering, Nankai University, Tianjin 300350, China*

Wen-Juan Tian − *Institute of Molecular Science, Shanxi University, Taiyuan 030006, China*

Jing-Ying Sun − *State Key Laboratory of Elemento-Organic Chemistry, Tianjin Key Lab for Rare Earth Materials and Applications, School of Materials Science and Engineering, Nankai University, Tianjin 300350, China*

Complete contact information is available at: https://pubs.acs.org/10.1021/jacs.4c03843

Notes

The authors declare no competing financial interest.

ACKNOWLEDGMENTS

This work was supported by the National Natural Science Foundation of China (nos. 223B2110, 92161102, and 22371140) and the Natural Science Foundation of Tianjin City (no. 21JCZXJC00140) and project 111 (B18030) from China (MOE).

REFERENCES

(1) Scharfe, S.; Kraus, F.; Stegmaier, S.; Schier, A.; Fässler, T. F. Zintl Ions, Cage Compounds, and Intermetalloid Clusters of Group

14 and Group 15 Elements. *Angew. Chem., Int. Ed.* **2011**, *50*, 3630−3670.

(2) Turbervill, R. S.; Goicoechea, J. M. From Clusters to Unorthodox Pnictogen Sources: Solution-Phase Reactivity of $[E_7]^{3-}$ (E = P−Sb) Anions. *Chem. Rev.* **2014**, *114*, 10807−10828.

(3) Dimaio, A. J.; Rheingold, A. L. Structural chemistry of transition metal complexes containing arsenic-arsenic bonds. *Chem. Rev.* **1990**, *90*, 169−190.

(4) Liu, C.; Popov, I. A.; Chen, Z.-F.; Boldyrev, A. I.; Sun, Z.-M. Aromaticity and Antiaromaticity in Zintl Clusters. *Chem.—Eur. J.* **2018**, *24*, 14583−14597.

(5) Critchlow, S. C.; Corbett, J. D. Homopolyatomic anions of the post transition elements. Synthesis and structure of potassium-crypt salts of the tetraantimonide(2-) and heptaantimonide(3-) anions, Sb_4^{2-} and Sb_7^{3-}. *Inorg. Chem.* **1984**, *23*, 770−774.

(6) Pan, F.-X.; Li, L.-J.; Wang, Y.-J.; Guo, J.-C.; Zhai, H.-J.; Xu, L.; Sun, Z.-M. An All-Metal Aromatic Sandwich Complex $[Sb_3Au_3Sb_3]^{3-}$. *J. Am. Chem. Soc.* **2015**, *137*, 10954−1095.

(7) Balázs, G.; Breunig, H. J.; Lork, E.; Mason, S. Neutron Diffraction Crystallography of *meso*-R(H)Sb-Sb(H)R and Reactions of R(H)Sb-Sb(H)R and RSbH2 (R = $(Me_3Si)_2CH$) Leading to Tungsten Carbonyl Complexes, Methylstibanes, and Antimony Homocycles. *Organometallics* **2003**, *22*, 576−585.

(8) Breunig, H. J.; Burford, N.; Rösler, R. Stabilization of a Pentastibacyclopentadienyl Ligand in the Triple-Decker Sandwich Complexes $[\{(\eta^5\text{-}1,2,4\text{-}{}^tBu_3C_5H_2)Mo\}_2(\mu,\eta^5\text{-}Sb_5)]$ and $[(\eta^5\text{-}1,2,4\text{-}{}^tBu_3C_5H_2)Mo(\mu,\eta^5\text{-}Sb_5)Mo(\eta^5\text{-}1,4\text{-}{}^tBu2\text{−}2\text{-}MeC_5H_2)]$. *Angew. Chem., Int. Ed.* **2000**, *39*, 4148−4150.

(9) Chitnis, S. S.; Burford, N.; Weigand, J. J.; McDonald, R. Reductive Catenation of Phosphine Antimony Complexes. *Angew. Chem., Int. Ed.* **2015**, *54*, 7828−7832.

(10) Wang, Y.; Zavalij, P.; Eichhorn, B. The *cyclo*-Sb_6 ring in the $[Sb_6(RuCp^*)_2]^{2-}$ ion. *Chem. Commun.* **2018**, *54*, 11917−11920.

(11) Reil, M.; Korber, N. A S_8-like $[Sb_8]^{8-}$ Zintl Anion in the Ammoniate $[K_{17}(Sb_8)_2(NH_2)]$ 17.5NH_3. *Z. Anorg. Allg. Chem.* **2007**, *633*, 1599−1602.

(12) Kesanli, B.; Fettinger, J.; Scott, B.; Eichhorn, B. Gas Phase, Solution, and Solid State Alkali Ion Binding by the $[NbE_8]^{3-}$ (E = As, Sb) Complexes: Synthesis, Structure, and Spectroscopy. *Inorg. Chem.* **2004**, *43*, 3840−3846.

(13) Kesanli, B.; Fettinger, J.; Eichhorn, B. Controlled Aggregation of ME_8^{n-} Binary Anions (M = Cr, Mo; E = As, Sb) into One-Dimensional Arrays: Structures, Magnetism and Spectroscopy. *J. Am. Chem. Soc.* **2003**, *125*, 7367−7376.

(14) Ruan, H.-P.; Wang, L.-L.; Li, Z.-Y.; Xu, L. Sb_{10}^{2-} and Sb_2^{2-} found in $[K(18\text{-crown-}6)]_6[Sb_{10}]$ $[Sb_4\{Mo(CO)_3\}_2]$·2en: two missing family members. *Dalton Trans.* **2017**, *46*, 7219−7222.

(15) Hanauer, T.; Korber, N. $[Sb_{11}]^{3-}$ and $[As_{11}]^{3-}$: Synthesis and Crystal Structure of Two New Ammoniates containing Trishomocubane-like Polyanions. *Z. Anorg. Allg. Chem.* **2006**, *632*, 1135−1140.

(16) García, F.; Less, R. J.; Naseri, V.; McPartlin, M.; Rawson, J. M.; Tomas, M. S.; Wright, D. S. Direct synthesis of the 1,2,3-$[C_6H_4P\cdots P\cdots P\cdots]$-anion, isoelectronic with the indenyl anion $[C_6H_4CH\cdots CH\cdots CH]$-. *Chem. Commun.* **2008**, 859−861.

(17) Jost, M.; Finger, L. H.; Sundermeyer, J.; von Hänisch, C. Simple access to ionic liquids and organic salts containing the phosphaethynolate (PCO^-) and Zintl (Sb_{11}^{3-}) anions. *Chem. Commun.* **2016**, *52*, 11646−11648.

(18) Bolle, U.; Tremel, W. $[Na(2,2,2\text{,-crypt})]_3[Sb_{11}]$, a salt containing the undecaantimonide(3−)anion. *J. Chem. Soc., Chem. Commun.* **1992**, 91−93.

(19) Zhai, J.; Xu, L. Synthesis and Crystal Structure of $[K(2,2,2\text{-crypt})]_3Sb_{11}$. *Chin. J. Struct. Chem.* **2011**, *30*, 1091−1094.

(20) Ganesamoorthy, C.; Wölper, C.; Nizovtsev, A. S.; Schulz, S. Synthesis and Structural Characterization of Magnesium-Substituted Polystibides $[(LMg)_4Sb_8]$. *Angew. Chem., Int. Ed.* **2016**, *55*, 4204−4209.

(21) Marczenko, K. M.; Chitnis, S. S. Bismuthanylstibanes. *Chem. Commun.* **2020**, *56*, 8015−8018.

(22) Breunig, H. J.; Rösler, R.; Lork, E. Sb_8R_4, R = $(Me_3Si)_2CH$-A Polycyclic Organostibane. *Angew. Chem., Int. Ed.* **1997**, *36*, 2237−2238.

(23) Schoo, C.; Bestgen, S.; Egeberg, A.; Klementyeva, S.; Feldmann, C.; Konchenko, S. N.; Roesky, P. W. Samarium Polystibides Derived from Highly Activated Nanoscale Antimony. *Angew. Chem., Int. Ed.* **2018**, *57*, 5912−5916.

(24) Schwamm, R. J.; Coles, M. P. Distibanes and Distibenes from Reduction of Sb(NON R) Cl by using Mg I Reagents. *Chem.—Eur. J.* **2019**, *25*, 14183−14191.

(25) Hanauer, T.; Aschenbrenner, J. C.; Korber, N. Dimers of Heptapnictide Anions: As_{14}^{4-} and P_{14}^{4-} in the Crystal Structures of $[Rb(18\text{-crown-}6)]_4As_{14}\cdot 6NH_3$ and $[Li(NH_3)_4]_4P_{14}\cdot NH_3$. *Inorg. Chem.* **2006**, *45*, 6723−6727.

(26) Haushalter, R. C.; Eichhorn, B. W.; Rheingold, A. L.; Geib, S. J. Oxidatively coupled polyarsenide clusters: synthesis and structures of $SnAs_{14}^{4-}$ and As_{22}^{4-}. *J. Chem. Soc. Chem. Commun.* **1988**, 1027−1028.

(27) Yue, X.-H.; Zhang, X.-W.; He, H.-M.; Qiao, L.; Sun, Z.-M. Synthesis, chemical bonding and reactivity of new medium-sized polyarsenides. *Chin. Chem. Lett.* **2024**, *35*, No. 108907.

(28) Min, X.; Popov, I. A.; Pan, F.-X.; Li, L.-J.; Matito, E.; Sun, Z.-M.; Wang, L.-S.; Boldyrev, A. I. All-Metal Antiaromaticity in Sb_4-Type Lanthanocene Anions. *Angew. Chem., Int. Ed.* **2016**, *55*, 5531−5535.

(29) Wang, Y.; Zavalij, P.; Eichhorn, B. $[(ZnSb_6)_2]^{4-}$: a new structure type for coupled norbornadiene-like subunits. *Chem. Commun.* **2017**, *53*, 11600−11602.

(30) Fleischmann, M.; Dielmann, F.; Gregoriades, L. J.; Peresypkina, E. V.; Virovets, A. V.; Huber, S.; Timoshkin, A. Y.; Balázs, G.; Scheer, M. Redox and Coordination Behavior of the Hexaphosphabenzene Ligand in $[(Cp^*Mo)_2(\mu,\eta^6:\eta^6\text{-}P_6)]$ Toward the "Naked" Cations Cu^+, Ag^+, and Tl^+. *Angew. Chem., Int. Ed.* **2015**, *54*, 13110−13115.

(31) Nikonov, G. I.; Kuzmina, L. G.; Howard, J. A. K. $Cp_2NbH_2SbPh_2$: Synthesis and Structure of the First Antimony-Substituted Niobocene. *Organometallics* **1997**, *16*, 3723−3725.

(32) Konchenko, S. N.; Virovets, A. V.; Apenina, S. A.; Tkachev, S. V. Synthesis and structure of the cubane type $[Fe_2Sb(CO)_5(\eta^5\text{-}C_5H_5)]_4$ cluster. *Inorg. Chem. Commun.* **1999**, *2*, 555−557.

(33) Gröer, T.; Palm, T.; Scheer, M. Novel Main Group-Transition Metal Cluster Compounds Incorporating Antimony, Iron and Cobalt. *Eur. J. Inorg. Chem.* **2000**, *2000*, 2591−2595.

(34) Adamo, C.; Barone, V. Toward reliable density functional methods without adjustable parameters: The PBE0 model. *J. Chem. Phys.* **1999**, *110*, 6158−6170.

(35) Weigend, F.; Ahlrichs, R. Balanced basis sets of split valence, triple zeta valence and quadruple zeta valence quality for H to Rn: Design and assessment of accuracy. *Phys. Chem. Chem. Phys.* **2005**, *7*, 3297−3305.

(36) Zubarev, D. Y.; Boldyrev, A. I. Developing paradigms of chemical bonding: adaptive natural density partitioning. *Phys. Chem. Chem. Phys.* **2008**, *10*, 5207−5217.

(37) Lu, T.; Chen, F.-W. Multiwfn: A multifunctional wavefunction analyzer. *J. Comput. Chem.* **2012**, *33*, 580−592.

https://doi.org/10.1021/jacs.4c03843
J. Am. Chem. Soc. XXXX, XXX, XXX−XXX